NOAA Technical Memorandum OAR PMEL-137

MODELING TSUNAMI INUNDATION FROM A CASCADIA SUBDUCTION ZONE EARTHQUAKE FOR LONG BEACH AND OCEAN SHORES, WASHINGTON

Angie J. Venturato[1,2]
Diego Arcas[1,2]
Utku Kânoğlu[3]

[1]NOAA/Pacific Marine Environmental Laboratory
Seattle, WA

[2]Joint Institute for the Study of the Atmosphere and Ocean (JISAO)
University of Washington, Seattle, WA

[3]Department of Engineering Sciences, Middle East Technical University,
Ankara, TURKEY

Pacific Marine Environmental Laboratory
Seattle, WA
July 2007

UNITED STATES DEPARTMENT OF COMMERCE

Carlos M. Gutierrez
Secretary

NATIONAL OCEANIC AND ATMOSPHERIC ADMINISTRATION

VADM Conrad C. Lautenbacher, Jr.
Under Secretary for Oceans
and Atmosphere/Administrator

Office of Oceanic and Atmospheric Research

Richard W. Spinrad
Assistant Administrator

NOTICE from NOAA

Mention of a commercial company or product does not constitute an endorsement by NOAA/OAR. Use of information from this publication concerning proprietary products or the tests of such products for publicity or advertising purposes is not authorized. Any opinions, findings, and conclusions or recommendations expressed in this material are those of the authors and do not necessarily reflect the views of the National Oceanic and Atmospheric Administration.

Contribution No. 2949 from NOAA/Pacific Marine Environmental Laboratory

Also available from the National Technical Information Service (NTIS)
(`http://www.ntis.gov`)

Contents

List of Figures

Modeling tsunami inundation from a Cascadia subduction zone earthquake for Long Beach and Ocean Shores, Washington

A.J. Venturato[1,2], D. Arcas[1,2], and U. Kânoğlu[3]

Abstract. The NOAA Center for Tsunami Research modeled tsunami inundation from a great Cascadia Subduction Zone earthquake for the coastal communities of Long Beach and Ocean Shores, Washington. A high-resolution numerical model was used to estimate tsunami propagation and inundation along the outer coast of southwest Washington. This effort was funded by the National Tsunami Hazard Mitigation Program via a grant from the Emergency Management Division of the Washington State Military Department.

1. Background

A great (moment magnitude, $M_w = 8.0$ or higher) Cascadia Subduction Zone (CSZ) earthquake represents the most devastating tsunami threat in the Pacific Basin to Washington State (National Science and Technology Council, 2005). Evidence from radiocarbon dating, Japanese historical records, and regional tribal accounts suggests that a great earthquake occurred along the CSZ in 1700 (Atwater *et al.* 1995; Satake *et al.*, 1996; Yamaguchi *et al.*, 1997). Petersen *et al.* (2002) estimate that another great CSZ earthquake has a 10–14 percent chance of occurring within the next 50 years.

As a result of this threat, Washington developed tsunami hazard and evacuation maps for several at-risk communities along the Pacific coast. Long Beach and Ocean Shores were mapped in 2000 as a result of finite element modeling studies from the Oregon Graduate Institute of Science and Technology (OGI). Since 2000, both peninsulas have been surveyed using high-resolution Light Detection and Ranging (LIDAR) systems to more accurately depict the topography. Additionally, improved grid development techniques (Venturato, 2005) are available to reduce horizontal and vertical control errors.

The Washington State Emergency Management Division provided a grant to the NOAA Center for Tsunami Research (NCTR) to reanalyze potential tsunami inundation at Long Beach and Ocean Shores due to a great CSZ earthquake. This effort includes:

- Using improved techniques to develop a new digital elevation model based on LIDAR and other updated elevation data.
- Using the finite difference Method of Splitting Tsunami (MOST) model instead of the original OGI finite element model known as ADCIRC.

[1]NOAA, Pacific Marine Environmental Laboratory, Seattle, WA, USA
[2]Joint Institute for the Study of the Ocean and Atmosphere (JISAO), Box 354235, University of Washington, Seattle, WA 98115-4235, USA
[3]Department of Engineering Sciences, Middle East Technical University, 06531 Ankara, TURKEY

- Using a M_w 9.1 CSZ earthquake with Washington asperity to match the "worst-case" tsunami source scenario developed in 2000.

The methodology and results of this effort are presented in the following sections. The results are compared to prior work and suggestions for further research are included.

2. Study Area

The study area lies along the southwest Washington coast within the Columbia River littoral cell (Fig. 1). The study region includes Ocean Shores, Ocean City, Oyhut, and Sampson in Grays Harbor County; and the communities of Long Beach, Klipsan Beach, Ilwaco, Seaview, Ocean Park, Surfside, Oysterville, and Nahcotta on the Long Beach peninsula in Pacific County (Fig. 2). Six State Parks, a National Wildlife Refuge, and several recreational areas also reside within the area.

The city of Ocean Shores covers most of the barrier beach that sits between the Pacific Ocean and Grays Harbor. Oyhut, Sampson, and Ocean City are small communities north of Ocean Shores. Ocean Shores has a population of 3,270 based on the 2000 U.S. Census (Grays Harbor County, 2005).

Tourism is the primary economic engine for the region with over three million visitors annually (Ocean Shores Chamber of Commerce, 2005). The peninsula has a 9.5-km beach on its western shore and a marina, passenger ferry, and municipal airport along its eastern shore. The Oyhut Wildlife Recreation Area consists of a saltwater marsh and resides on the southeast corner of the peninsula.

The Long Beach Peninsula serves as a barrier between the Pacific Ocean and the Willapa Bay estuary. It has the longest (45 km) natural beach in the United States. The region's economy consists primarily of tourism, shellfish harvesting, recreational fishing, and logging. The Port of Peninsula sits within Willapa Bay, and the Port of Ilwaco lies within the Columbia River. Long Beach and Ilwaco are the largest communities on the peninsula, with populations of 1,340 and 945, respectively (Pacific County, 2003).

2.1 Coastal Morphology

The Columbia River littoral cell is a highly dynamic region that experiences alternating patterns of progradation and erosion due to longshore sediment transport, tidal forcing, and intense winter storms (Peterson *et al.*, 1999). Additionally, geologic evidence has shown that past great Cascadia earthquakes have caused catastrophic beach retreat due to coseismic subsidence (Atwater, 1987; Doyle, 1996). The natural episodic pattern of progradation and retreat have been altered in recent times (1870 to present) due to anthropogenic development.

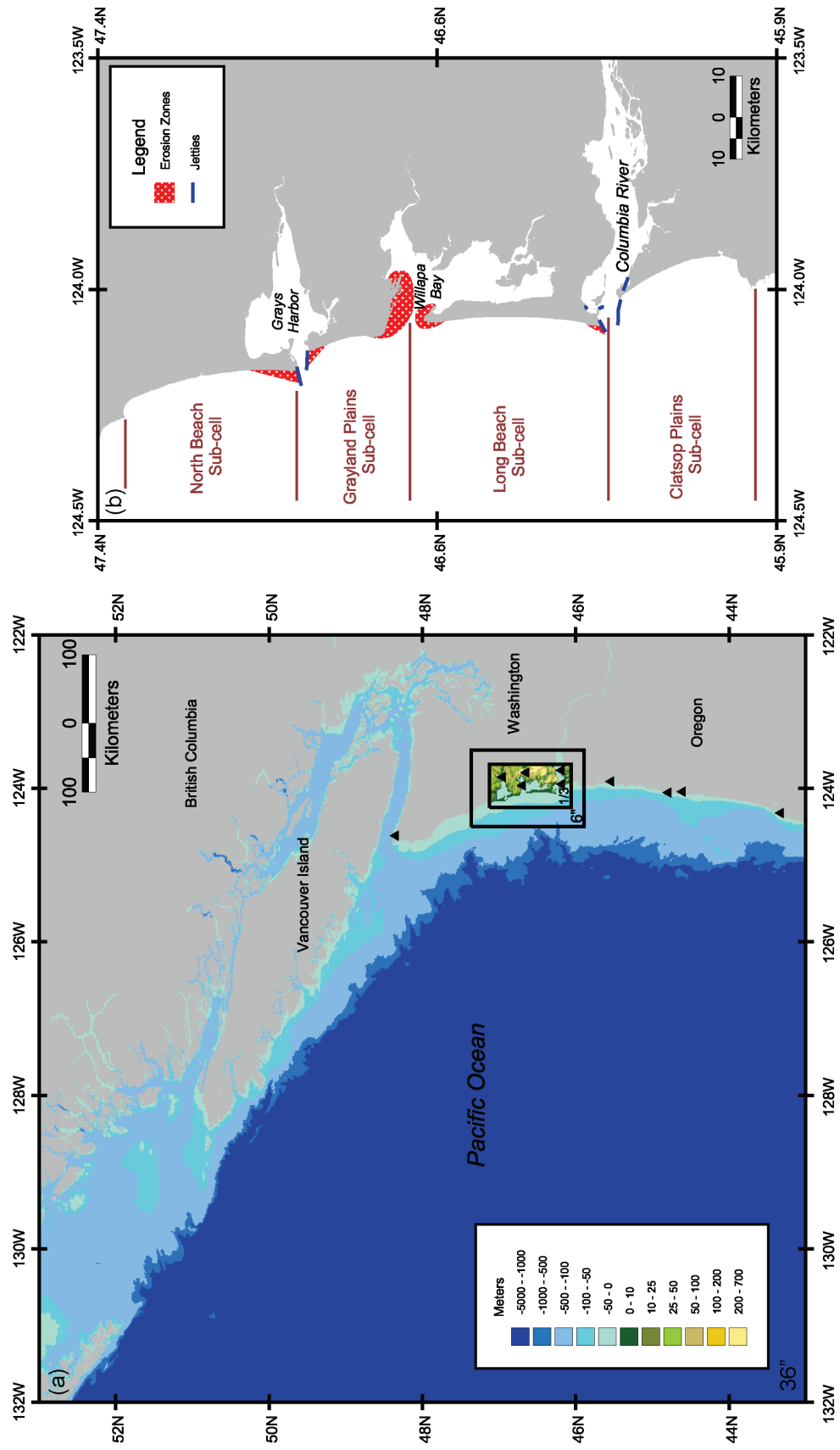

Figure 1: (a) Extent and resolution of each digital elevation model (DEM) used in the study. The low-resolution DEMs consist of bathymetric depth values only. The high-resolution DEM consists of bathymetry and topography. The triangles depict the water-level stations used to convert vertical values to Mean High Water (Mofjeld *et al.*, 2004). (b) The Columbia River littoral cell. The Long Beach peninsula sits within the Long Beach sub-cell, and Ocean Shores lies within the North Beach sub-cell.

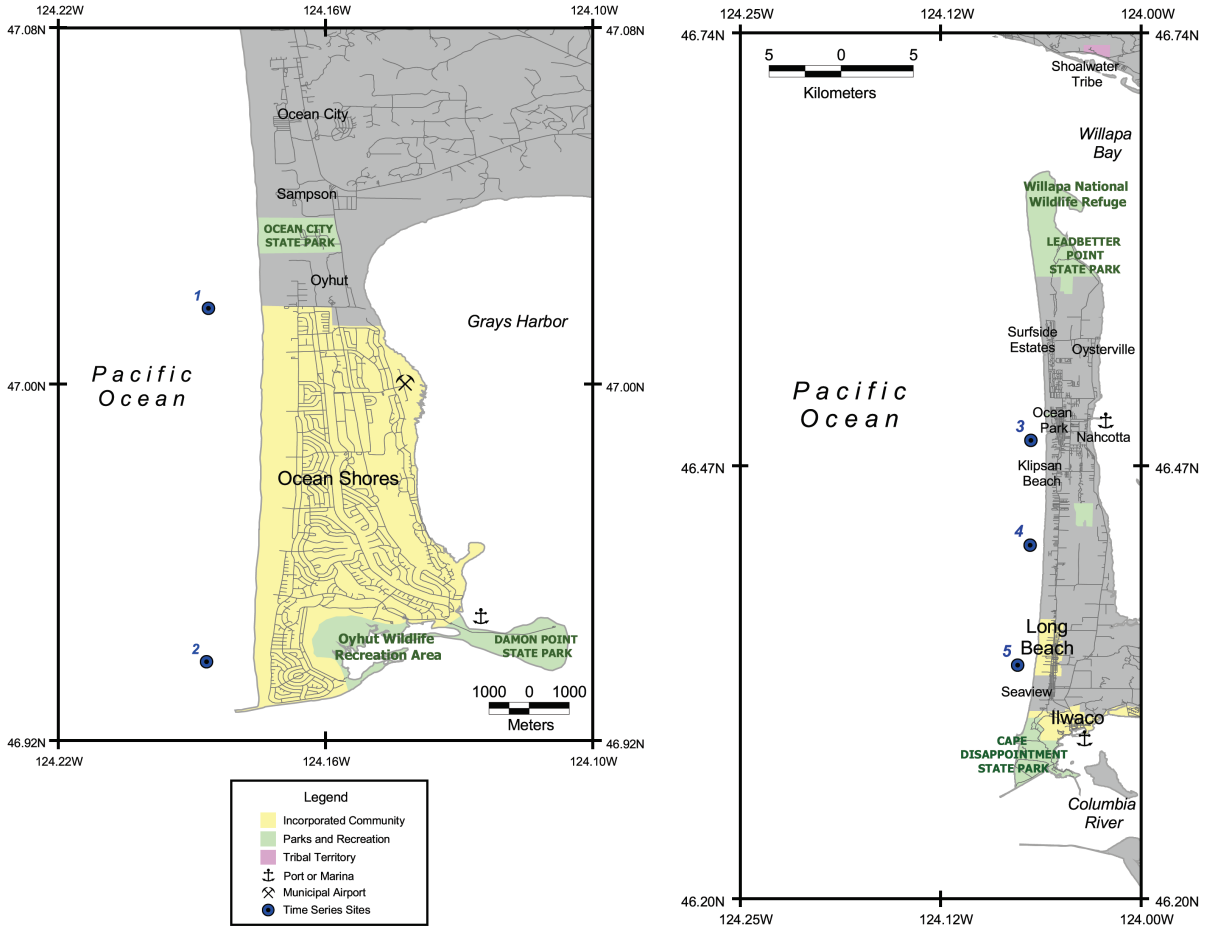

Figure 2: Study area for tsunami inundation. Details of the (a) Ocean Shores region and (b) the Long Beach peninsula. Modeled time series locations are depicted as blue circles and coincide with selected locations from Walsh *et al.* (2000) (Fig. 6).

The Columbia River littoral cell consists of four sub-cells that are divided by tidal inlets (Fig. 1b). Ocean Shores and the Long Beach Peninsula lie within the North Beach and Long Beach sub-cells, respectively. Before the early 1900s, these sub-cells experienced natural shoreline progradation of approximately 0.1–1.2 m/yr due to longshore sediment transport from the Columbia River (Woxell, 1998). In the late 1800s and early 1900s, jetties were installed at the mouth of the Columbia River and the entrance to Grays Harbor to restrict inlet flow for navigation.

These jetties had a significant impact on the accretion rates of the North Beach and Long Beach sub-cells. Initially, both sub-cells experienced rapid progradation along their respective barrier beaches (4–6 m/yr) due to the jetties trapping sediment along their outer flanks (Kaminsky *et al.*, 1999). Since the construction of dams in the Columbia River and the start of dredging and disposal maintenance programs throughout the littoral cell in the mid-1900s, each sub-cell has experienced high levels of erosion (Peterson *et*

al., 1999). Additionally, the lack of sand has led to deepening waters offshore, making these beaches more susceptible to rapid beach retreat during intense storms and seismic events.

Both Ocean Shores and the Long Beach peninsula experience beach alteration due to these anthropogenic effects. Several erosion hotspots (Fig. 1b) are threatening state parks, natural habitat, and coastal development along each barrier beach (Washington State Department of Ecology, 2007).

3. Tsunami Source

Tsunami generation by a rupture along the CSZ is considered for this study. The earthquake would create onshore subsidence and large offshore uplift generating an intense tsunami with two fronts: one directed toward the Pacific Northwest coast as evidenced by geologic evidence (Atwater *et al.*, 1995), and the other directed offshore as evidenced by historic Japanese records (Satake *et al.*, 1996).

Priest *et al.* (1997) and Myers *et al.* (1999) developed six scenarios that consider various slip distributions along locked and transition zones along the CSZ to match paleoseismic evidence. Walsh *et al.* (2000) added additional coseismic slip, or an asperity, offshore of Washington to one of these scenarios (Scenario 1A) based on the presence of low-gravity anomalies detected by satellite, bathymetry, and seismic profiling (Wells and Blakely, 2003). Scenario 1A plus the Washington asperity is considered the worst-case scenario for tsunami inundation at Long Beach and Ocean Shores.

The 4.5-m asperity was generated using an elliptical Gaussian distribution centered at 47.324°N, 124.94°W. The resulting slip distribution corresponds with a M_w 9.1 earthquake with a total uplift (asperity amplitude plus Scenario 1A deformation) of 6 m in the high-slip area (Fig. 3). Additional parameters are provided in Table 1.

Table 1: Tsunami source parameters (CSZ Scenario 1A plus Washington asperity). The slip distribution is displayed in Fig. 3.

Parameter	**Value**
Rupture length along fault	1050 km
Rupture width	70 km
Average slip along fault	17.5 m
Moment magnitude	9.1
Asperity location	47.324°N, 124.94°W
Asperity amplitude	4.5 m
Elliptical axis orientation	0°
Elliptical semi-major axis	38.45 km
Elliptical semi-minor axis	25.63 km

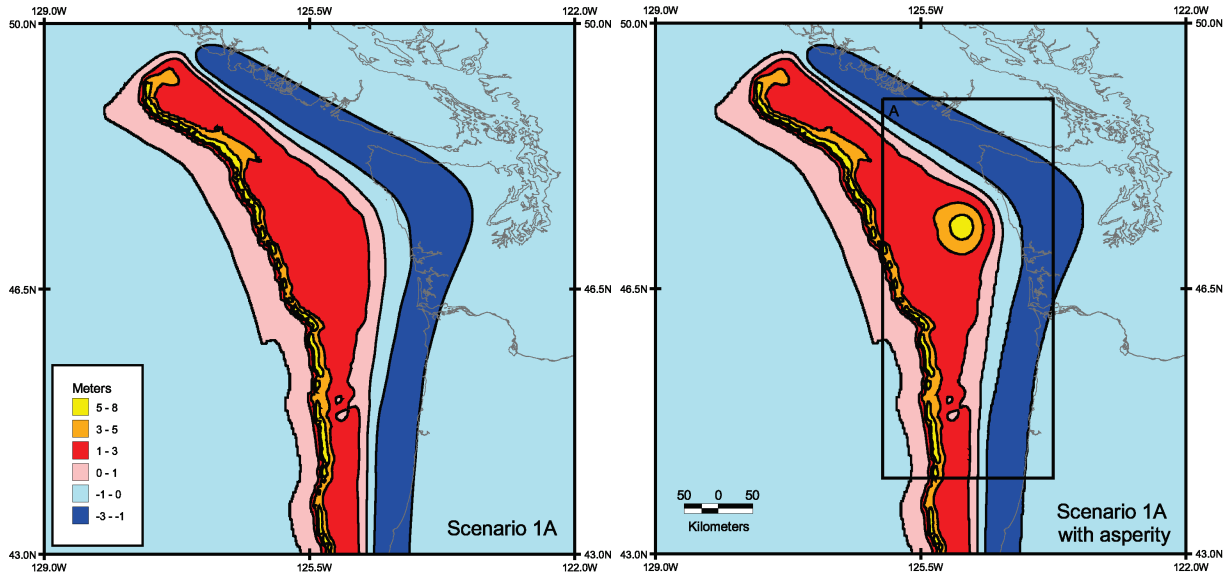

Figure 3: Initial deformation. The left panel shows the original Scenario 1A deformation (Myers *et al.*, 1999; Priest *et al.*, 1997). The right panel shows the initial deformation used in this model study, Scenario 1A with Washington asperity (Walsh *et al.*, 2000). The right panel also overlays the extent of model grid A.

4. Tsunami Model

The finite-difference long wave approximation MOST model is used in this study to compute tsunami propagation and inundation (Titov and González, 1997). Though a robust, but less accurate, version of MOST is used for tsunami forecasting, this study uses the more accurate, original version of MOST. The original model has been extensively tested against analytical, laboratory, and field data in accordance with NOAA tsunami modeling standards (Synolakis *et al.*, 2007; Titov and Synolakis, 1998; Titov and González, 1997). Titov *et al.* (2003) details the application of the MOST model for a tsunami hazard mapping project. Model parameters and grid development methods for this study are summarized below.

The MOST model requires three nested computational grids to calculate tsunami wave dynamics. The grids interact with each other by passing wave height and velocity information between nodes along their intersecting boundaries. The A grid passes data to the B grid, which in turn passes it to the C grid, and vice versa (Fig. 4). The A grid is relatively coarse, since fewer node points are needed to resolve tsunami waves in deep water. As the wave travels into shallower water, more node points are needed due to shorter wavelengths; thus, the B and C grids are of higher resolution.

The A and B grids are used to compute wave propagation only. Simulated waves in the A and B grids reflect off a pre-determined offshore boundary.

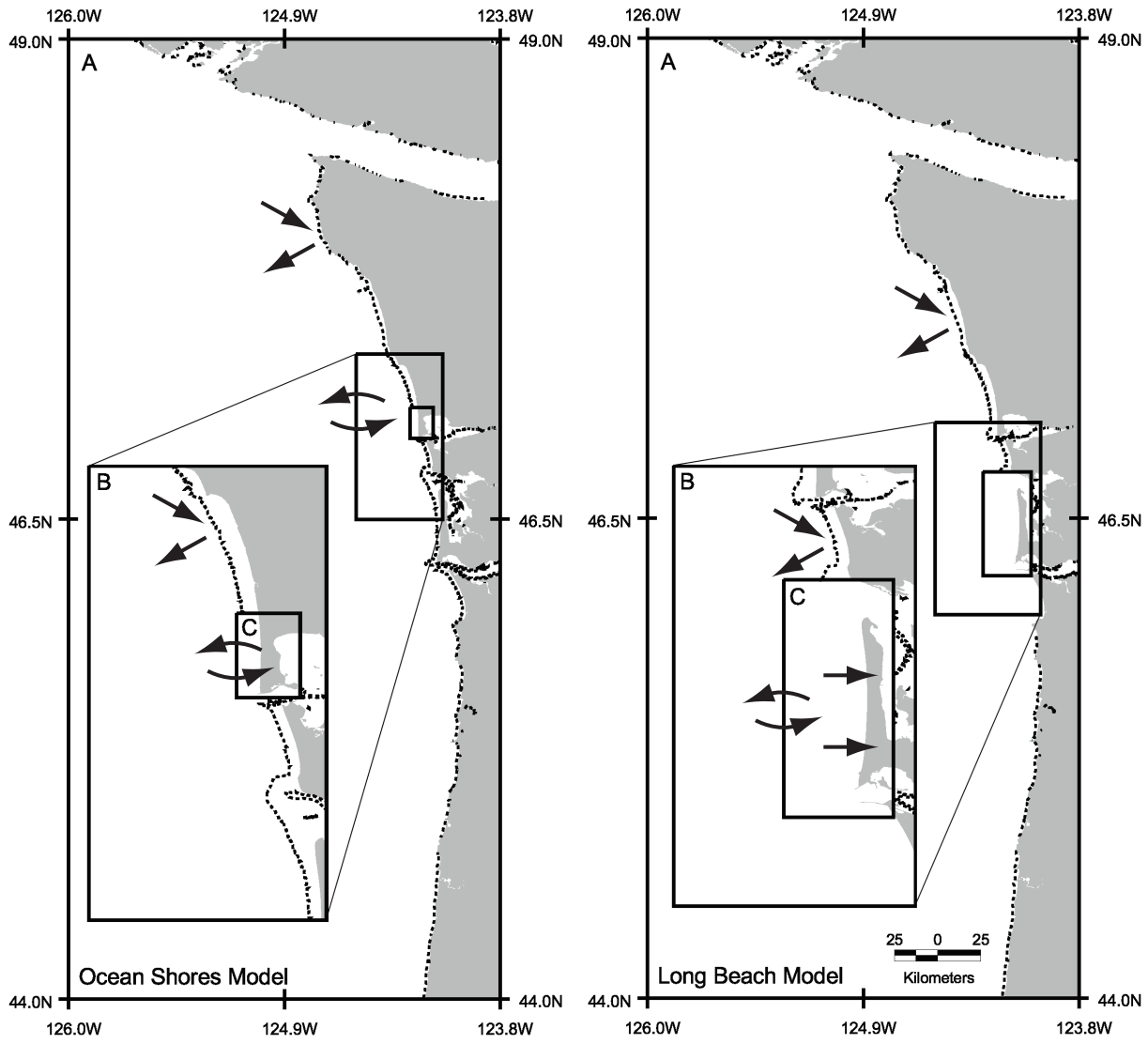

Figure 4: Extent of model grids for Ocean Shores (left panel) and Long Beach (right panel). Tsunami inundation is computed in the C grid and wave propagation is computed in all three grids. Each inset shows the details of the reflection boundary within the B grid. The dashed line represents the reflection boundary depth (Table 3) used for each simulation. The arrows represent wave propagation and reflection between grids.

The boundary is chosen to limit model instabilities that may occur due to the seafloor being bared during wave recession. The C grid is used to compute wave propagation and inundation on land; thus, no reflection boundary is implemented in this grid (Fig. 4). In order to compute tsunami inundation accurately, high-resolution bathymetry and topography are required in the C grid.

4.1 Digital Elevation Model Development

Three digital elevation models (DEMs) were developed for this study (Fig. 1a). Bathymetric, topographic, and shoreline data were collected from various agencies and converted to standard units based on model specifications (Table 2). Because the MOST model does not include tidal dynamics, Mean High Water was used as the baseline vertical datum to simulate the inundation scenario at high tide. This is a relatively conservative value for the background water level, since the most probable level for the maximum heights of large tsunamis along the Pacific coast are closer to Mean Sea Level (Mofjeld *et al.*, 2007). Vertical datum transformations were applied using linearly interpolated values from official National Ocean Service (NOS) datums at water-level stations (Fig. 1a) along the Pacific Northwest coast (Mofjeld *et al.*, 2004).

Data were analyzed and combined using methods described in Venturato (2005). Data sources used to develop the DEMs are provided in Appendix A. As in other tsunami inundation studies, the vegetation and manmade structures were removed from the topography to produce a "bald-earth" DEM.

The DEMs were created using a simple method of Delauney triangulation and nearest neighbor interpolation. A spatial analysis was performed to ensure quality from original data sources and consistency between DEMs. The 1/3-, 6-, and 36-arc-second DEMs were converted to ASCII raster grids for use in the tsunami model.

4.2 Model Setup

The DEMs were clipped and resampled to reduce the number of computations required in the MOST model (Fig. 4, Table 3). A smoothing algorithm was also applied to the computational grids to maintain model stability by reducing potential discontinuities due to single-node cells (i.e., offshore islands). The model grids are then adjusted for coseismic displacement by adding the deformation field (Fig. 3) to the vertical values in the grid.

As described previously, the gridded land surface does not contain vegetation or man-made structures. In reality, these obstacles may alter the amount and pattern of tsunami inundation. Thus, the model includes a conservative friction coefficient to add roughness to the land surface (Manning parameter, $n = 0.025$). Though this value may be conservative, it represents a reasonable estimate given the lack of proven scientific studies regarding tsunami forces on structures.

5. Model Results

5.1 Offshore Dynamics

The CSZ source creates 1–2 m of subsidence onshore with significant uplift offshore (Fig. 3). This generates a leading depression wave along the entire

Table 2: Baseline DEM parameters.

Coordinate system	Geographic decimal degrees
Horizontal datum	World Geodetic System of 1984 (WGS84)
Vertical datum	Mean High Water
Vertical units	Meters

Table 3: MOST model parameters.

Parameter	**Long Beach**	**Ocean Shores**
Grid resolution (arc-seconds)	A: 36, B: 6, C:1	A: 36, B: 6, C: 1
Offshore reflection boundary depth for A and B grids (meters)	15	13
Land depth for inundation (meters)	0.1	0.2
Friction coefficient, n	0.025	0.025
Time step (seconds)	0.6	0.6
Model simulation time (hr)	7.5	7.5

coastal region. This is followed by a large wave crest that strikes the northern Washington coast 19 min after tsunami generation (Fig. 5). The initial wave crest progresses along the coast from north to south, striking the study region at approximately 30 min after generation.

A second wave crest created from the ruptured fault builds upon the initial asperity-induced wave. This leads to maximum wave crest amplitudes of 5–6 m along the coast of Ocean Shores and 7–8 m along the Long Beach peninsula. The initial wave crest is followed by a 3.3-m trough along the Long Beach peninsula 45 min after generation. A much larger trough (10 m) bares the seafloor 60 min after generation along Ocean Shores. The largest trough (∼6 m) along the Long Beach peninsula occurs 1 hr, 50 min after generation.

Complicated wave dynamics occur along the southwest Washington coast after the initial wave train. This is due to wave scattering and reflection from regional topography. Instabilities in the velocity field start to develop after 3.5 hr of simulation time. Thus, the time series are displayed for the first 3 hr only (Fig. 6). However, given the potential for wave trapping along the continental shelf, tsunami waves are likely to continue over several hours (Mofjeld *et al.*, 2000).

As described earlier, this model simulation is based on the great Cascadia earthquake that is estimated to have occurred at 0500 UTC on 27 January 1700 (Satake *et al.*, 1996). Tidal hindcasts suggest that the tsunami reached the study area at low tide (Mofjeld *et al.*, 1997). The modeled propagation was calculated at high tide to produce a probable worst-case scenario. Thus, the simulated wave heights are higher than would be predicted at low tide.

High tsunami current speeds (>1.5 m/s) occur throughout the region. Since the model does not dynamically include tidal currents, the current speeds may be more substantial if the tsunami occurred during flood tide. Variable subtidal water levels from El Niño/Southern Oscillation or storm events that may also influence tsunami wave heights and currents are not included in this model.

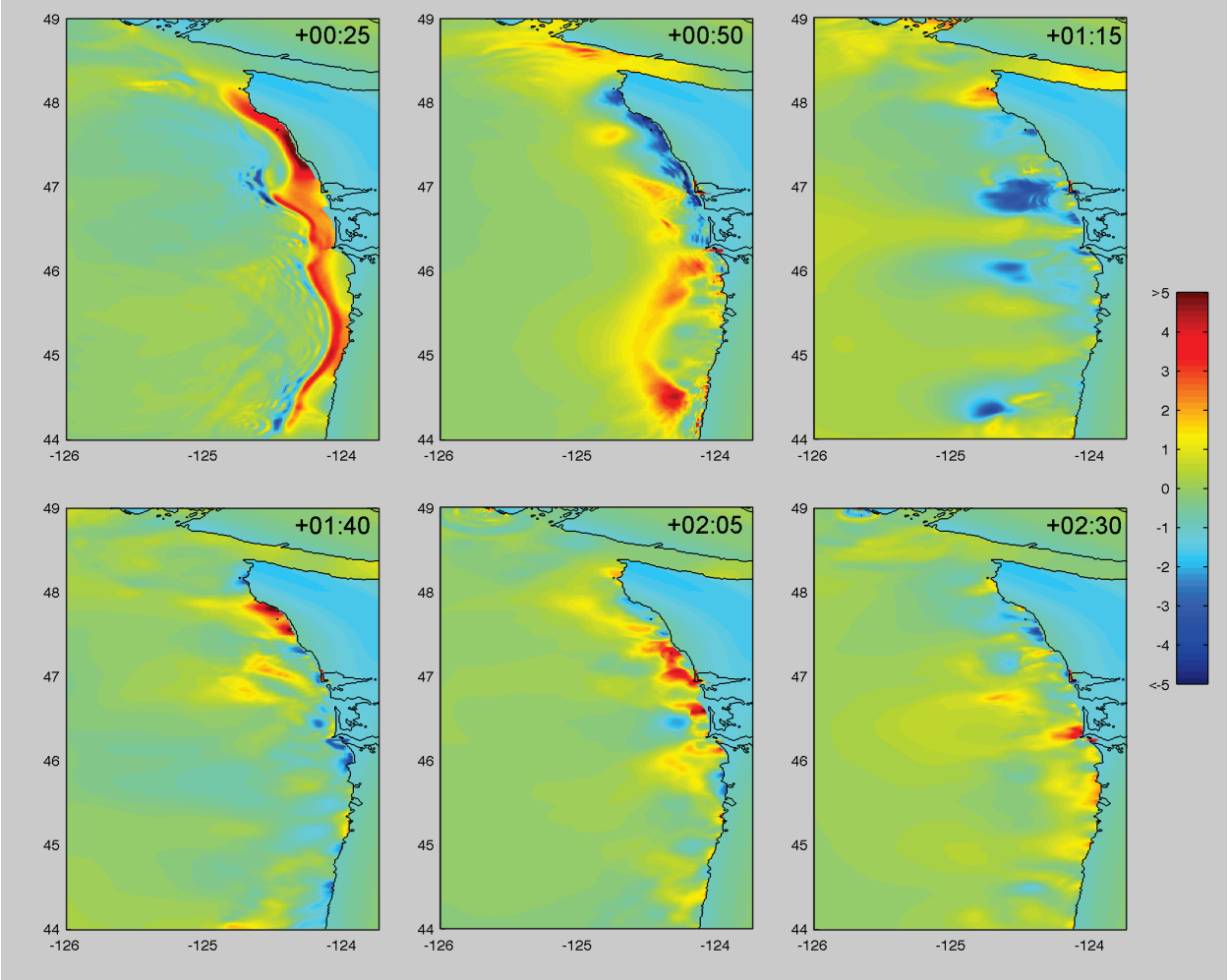

Figure 5: Snapshots of modeled tsunami propagation. Frames are in 25-min intervals with wave heights in meters.

5.2 Inundation Details

The model predicts extensive inundation along all low-lying regions of the study area. This is expected due to the initial subsidence (∼1 m at Ocean Shores and ∼1.4 m at Long Beach), the large offshore wave heights, and the relatively flat topography of both peninsulas. Regional inundation details are described below.

Due to the constraints of the inundation grids, the model does not consider the full extent of wave propagation within the Grays Harbor and Willapa Bay estuaries. High frequency waves propagating out of the inundation grid and into the estuary are not adequately resolved by the coarser B grid. As a consequence, the internal wave dynamics in the estuary may not be accurately resolved, and reflections affecting the eastern side of each peninsula may not be adequately modeled. Wave propagation within these

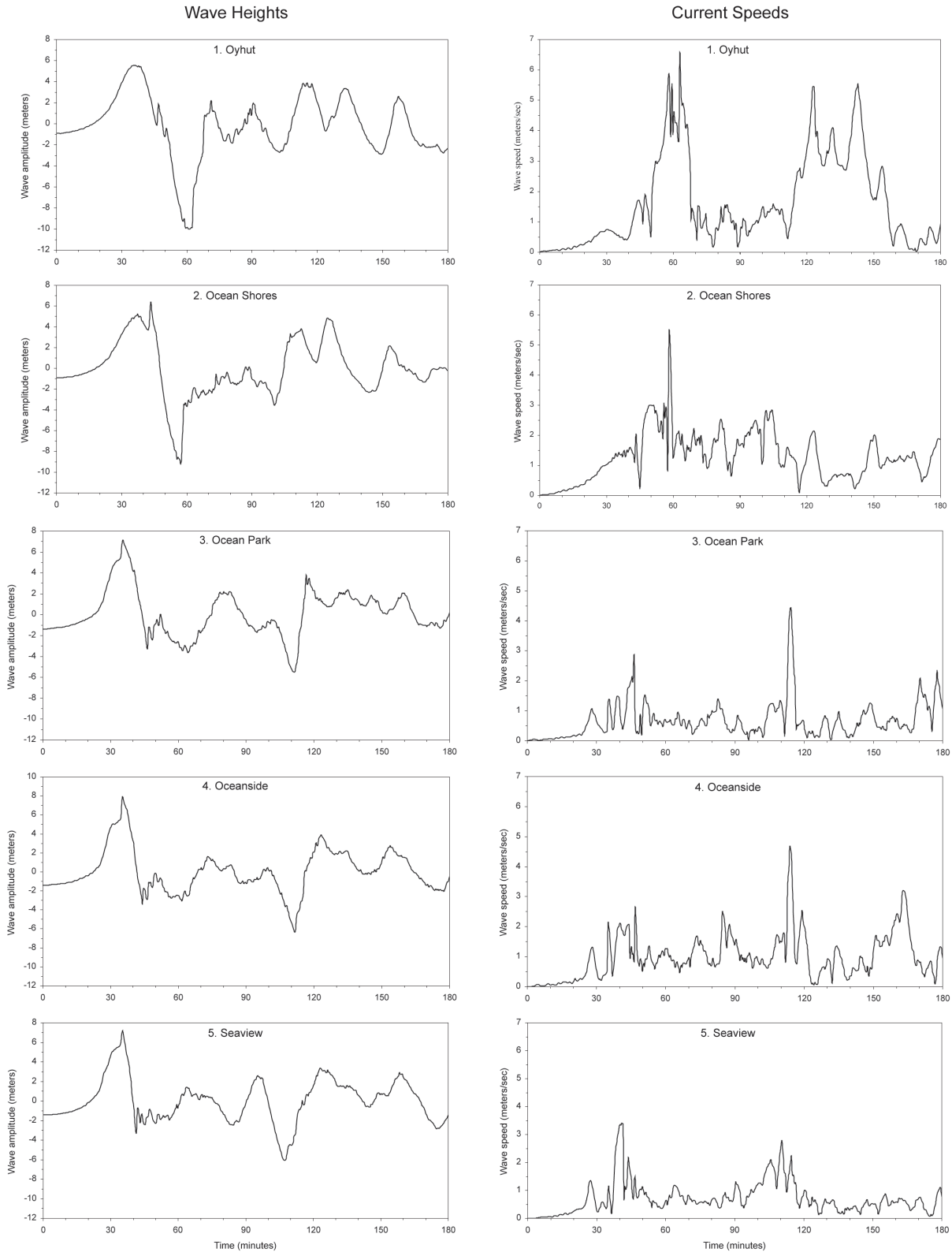

Figure 6: Time series of wave heights and current speeds at select sites of the study region. Figure 2 shows the locations of these sites.

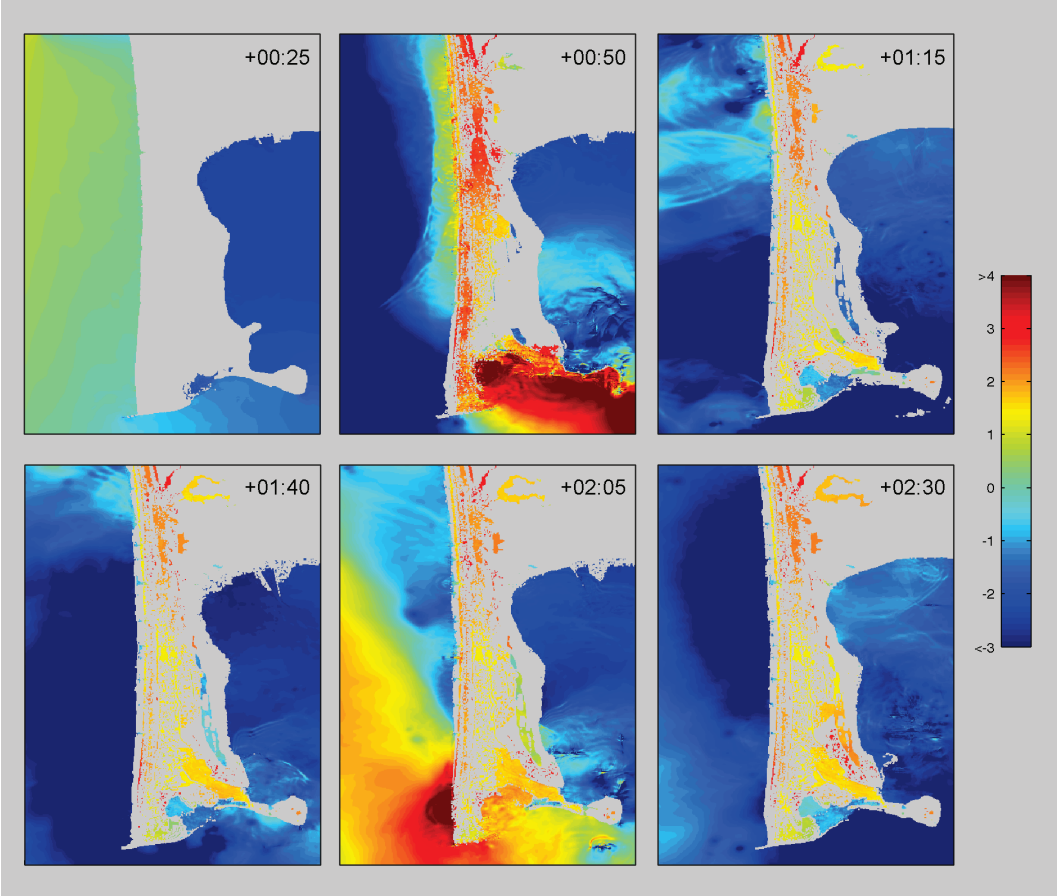

Figure 7: Modeled tsunami inundation at Ocean Shores. Snapshots are in 25-min intervals starting near the time of initial inundation. Wave heights are in meters with respect to Mean High Water.

regions are additionally restricted due to the reflection boundaries imposed on the A and B grids (Fig. 4).

5.2.1 Ocean Shores

Most of the flooding along the Ocean Shores region is due to the initial wave train generated by the tsunami source (Fig. 7). First, a large 5-m wave crest produced by the asperity strikes the outer coast approximately 30 min after generation. As that wave begins to recede over the next 15 min, a second wave crest (6.3 m) strikes the southern tip and cascades up the peninsula. This phenomena is followed by a 9-m wave trough that bares the seafloor approximately 1 hr after generation.

The first wave train causes extensive inundation along the entire peninsular region. The initial wave crest completely overtops the peninsula where Oyhut and Ocean City Park lie. The Wildlife Recreation Area and Damon Point State Park are also overtopped with maximum flow depths of 5–8 m (Fig. 8).

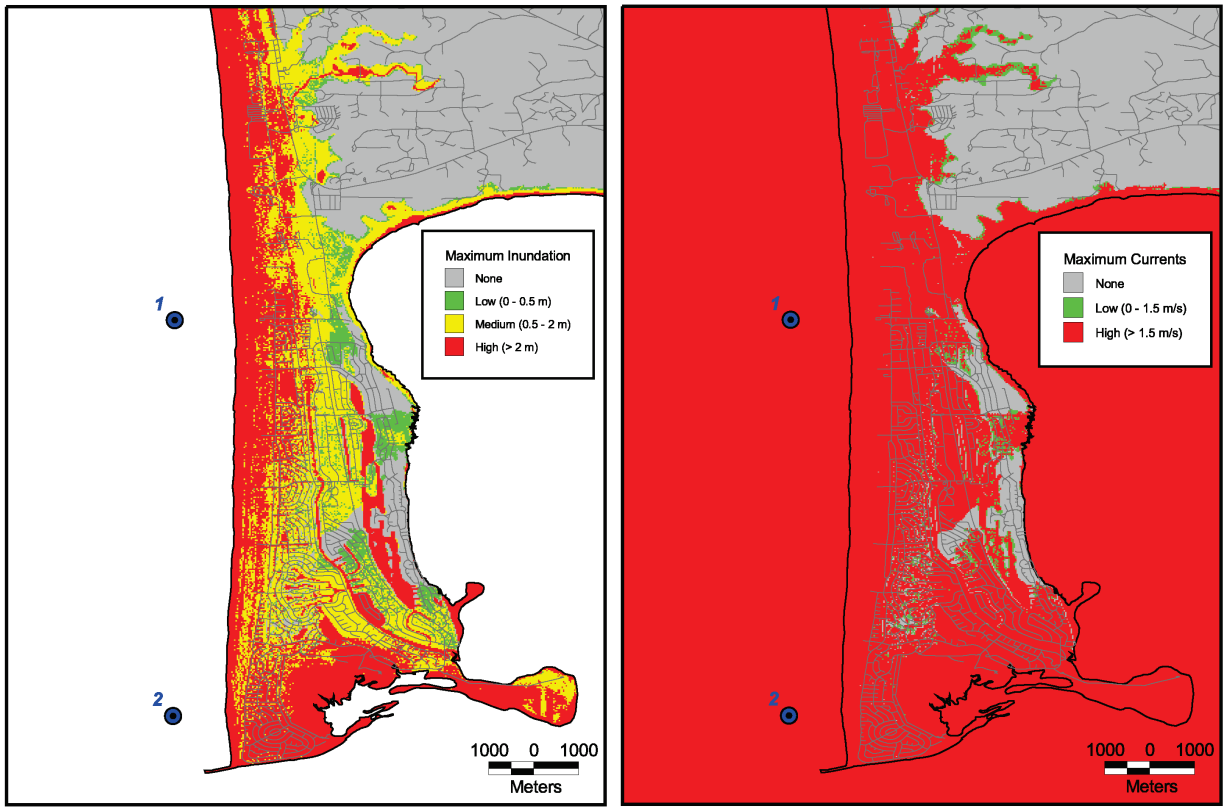

Figure 8: Maximum inundation (left panel) and current speeds (right panel) for the Ocean Shores region. Time series sites (Fig. 6) are displayed as blue circles.

Ocean Shores sees extensive damage as the initial wave propagates across the community. The second largest wave occurs 2 hr after generation, with several damaging waves in between. These later waves are primarily due to reflection and refraction along the coast and offshore along the continental shelf margin. Maximum flow depths reach 6–8 m along the barrier beach.

Extreme current speeds (5.5–6.5 m/s) occur during the first wave train. Oyhut continues to experience large tsunami current speeds over the simulation run; smaller, but still dangerous, velocities occur at Ocean Shores. The marina experiences maximum current speeds of 4–6 m/s.

5.2.2 Long Beach Peninsula

Like Ocean Shores, Long Beach peninsula flooding is primarily due to the first wave train (Fig. 9). The initial wave crest strikes the beach 30 min after generation and builds to an approximate 8-m peak as other secondary waves catch up. Maximum flow depths average 7–8 m along the beach barrier. The beach barrier provides some protection as the wave propagates and dissipates into coastal communities. However, all communities along the western shores are completely inundated with maximum flow depths averaging 1–3 m (Fig 10).

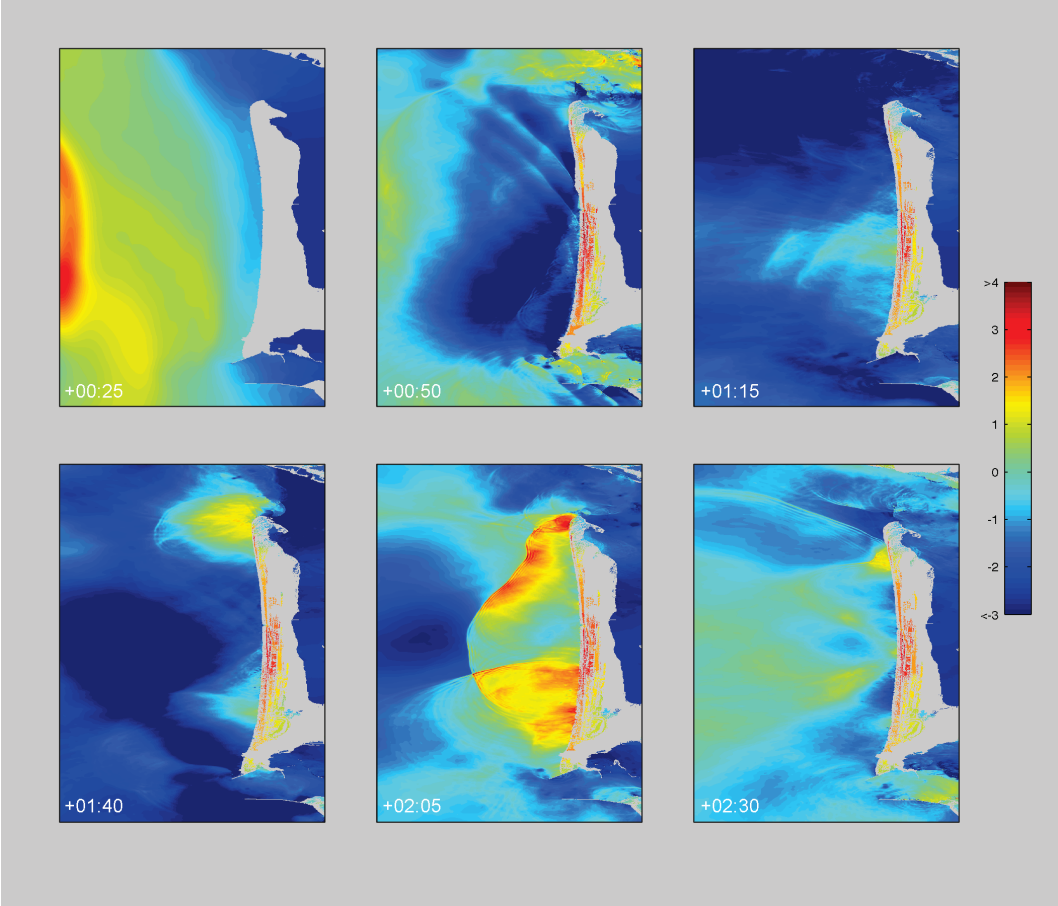

Figure 9: Modeled tsunami inundation of the Long Beach peninsula. Snapshots are in 25-min intervals. Wave heights are in meters with respect to Mean High Water.

Extensive inundation also occurs along low-lying regions of the Willapa National Wildlife Refuge and both major state parks. This simulation shows little inundation along the eastern coast. Maximum tsunami current speeds reach up to 5 m/s along the barrier beach, and 2.5 m/s at the Port of Ilwaco.

Modeled wave dynamics along the Long Beach peninsula display interesting results. The first wave crest has the largest amplitude, but is followed by a relatively minor trough (Fig. 6). The deepest trough (5–6 m) precedes the second largest wave crest. Thus, the largest tsunami current speeds (4.5–5 m/s) occur approximately 1.8 hr after generation at Ocean Park and Oceanside.

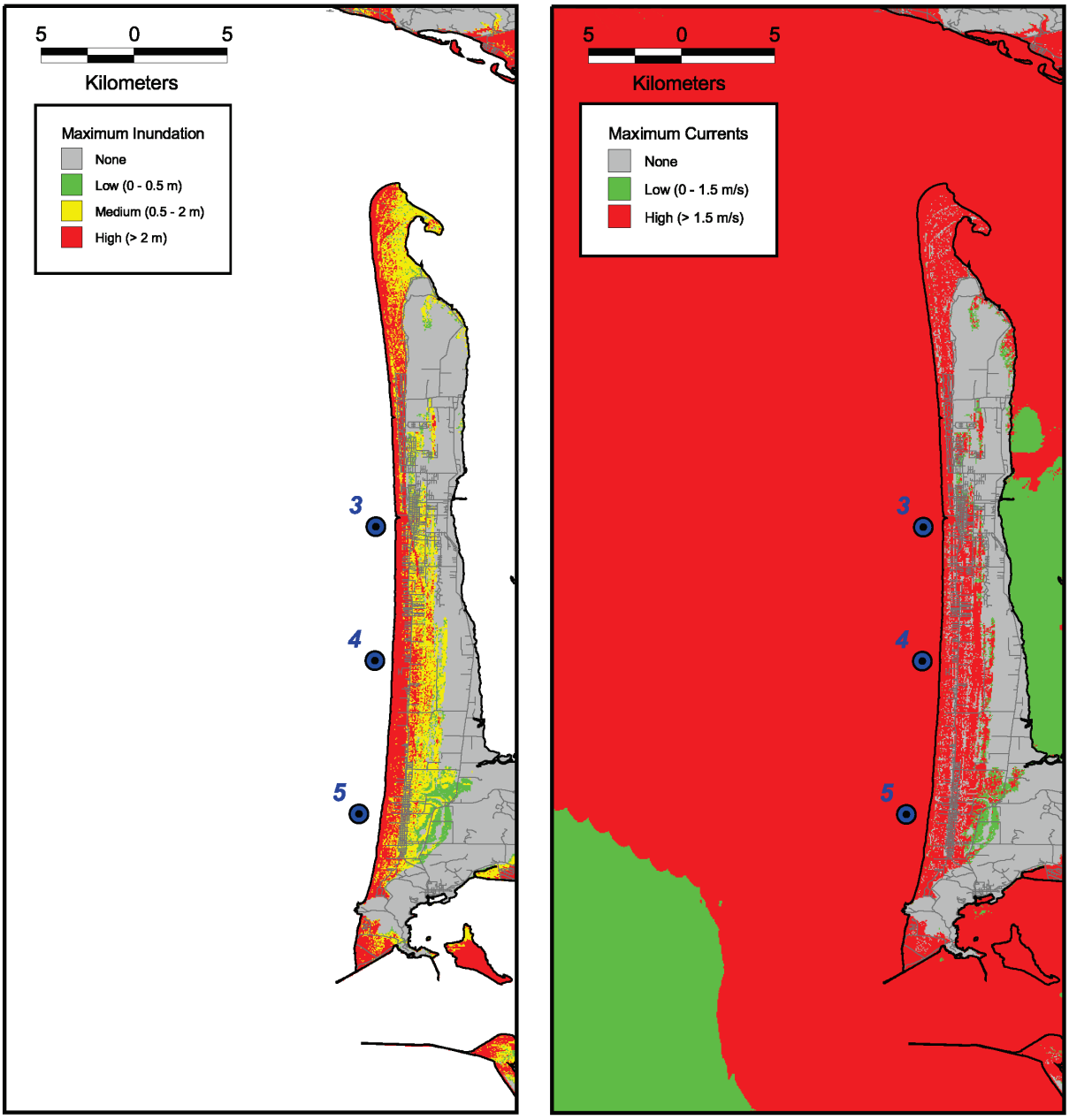

Figure 10: Maximum inundation (left panel) and current speeds (right panel) for the Long Beach peninsula. Time series sites (Fig. 6) are displayed as blue circles.

6. Discussion

6.1 Potential Sources of Error

The MOST model used in this study has been extensively tested against analytical solutions, laboratory measurements, and field data (Titov and González, 1997; Titov and Synolakis, 1998). Since the model performs well with all of the benchmark cases described in Synolakis *et al.* (2007), potential errors are limited to the quality of the model initialization parameters, the initial deformation of the tsunami source, and the DEM.

The setup of the initial conditions for these simulations may produce potentially substantial error in terms of the amount of inundation. As described in the previous sections, the DEMs were clipped into smaller A, B, and C grids to reduce computational time. The A grid does not cover the entire extent of the initial deformation (Fig. 3). Thus, some of the potential tsunami energy is not being considered. Though this may not affect the maximum inundation from the main energy beam, there are likely additional effects from coastal reflection and scattering that are lost.

To stabilize model simulation, the reflection boundaries and inundation depths for each simulation are different (Table 3). The offshore depth of these boundaries may be causing unrealistic wave reflection patterns along the outer coast (Fig. 4). This may influence the timing, amplitude, and direction of later waves.

Additionally, the boundaries of the inundation grid are not adequately modeling internal waves in the estuarine regions. This may significantly affect the amount and pattern of inundation on land.

Ideally, the C grid would be extended to cover Willapa Bay and Grays Harbor to fully account for the influence of these estuaries on tsunami inundation (Fig. 11). Also, the reflection boundaries would be based on a depth (1–2 m) that is much closer to the actual coastline. A new model version is currently being tested to allow for extended grids and shallow reflection boundaries.

6.1.1 Limitations of the tsunami source

Tsunami generation depends on the initial deformation of the earthquake. Priest *et al.* (1997) and the Tsunami Pilot Study Working Group (2006) considered several CSZ deformation scenarios that adequately explore levels of variation in line with paleoseismic evidence. However, the next CSZ earthquake could have a substantially different slip distribution than the modeled source and may be associated with tsunamigenic submarine landslides (Goldfinger *et al.*, 1992). Thus, the source represents the largest uncertainty in the simulation.

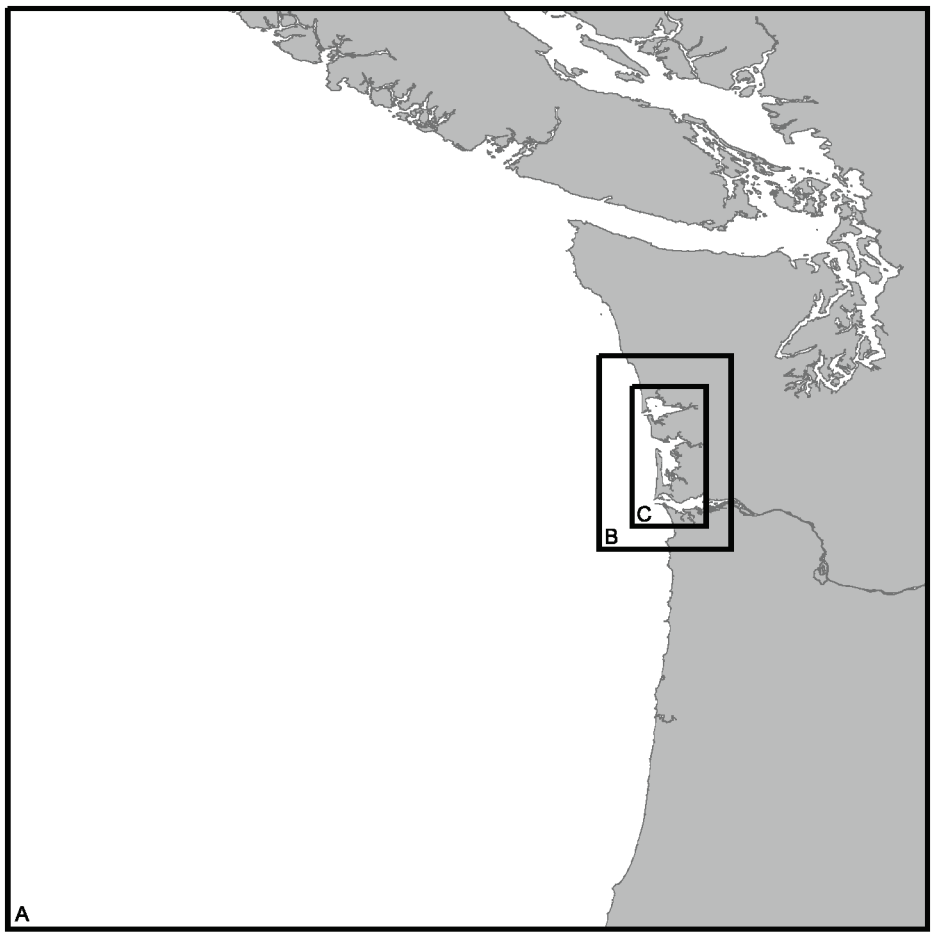

Figure 11: Proposed grid extent to reduce potential errors in the model setup. The A grid should be extended to include the entire initial deformation field. The C grid should be extended to include both Grays Harbor and Willapa Bay.

The location of the asperity within the rupture area has a significant effect on the directivity of the tsunami energy, and subsequently, on the maximum inundation at Long Beach and Ocean Shores. Priest *et al.* (1997) saw similar effects when simulating a different asperity further south that magnified tsunami energy along the Oregon coast. Other regional asperities within the low-gravity forearc basins should also be investigated to look at the range of tsunami energy patterns.

6.1.2 Limitations of the DEM

A high quality DEM is necessary to properly model tsunami wave dynamics and inundation onshore. A number of different factors can contribute to DEM error, including known quantitative errors due to datum conversion and unknown inherent errors produced by combining multiple data sources. Table 4 estimates the total known error for the high-resolution DEM as described in Venturato (2005).

Table 4: Estimates of root mean square error based on limited known quantitative values for the high-resolution model (Venturato, 2005).

Error Type	Horizontal Error (m)	Vertical Error (m)
Projection/datum conversion range	0.35–0.45	0.05–0.40
Comparison with vertical control	N/A	0.14–1.80
Comparison with original data sources	0.80–10	0.01–1.24
Total known quantitative error	1.15–10.45	0.20–3.44

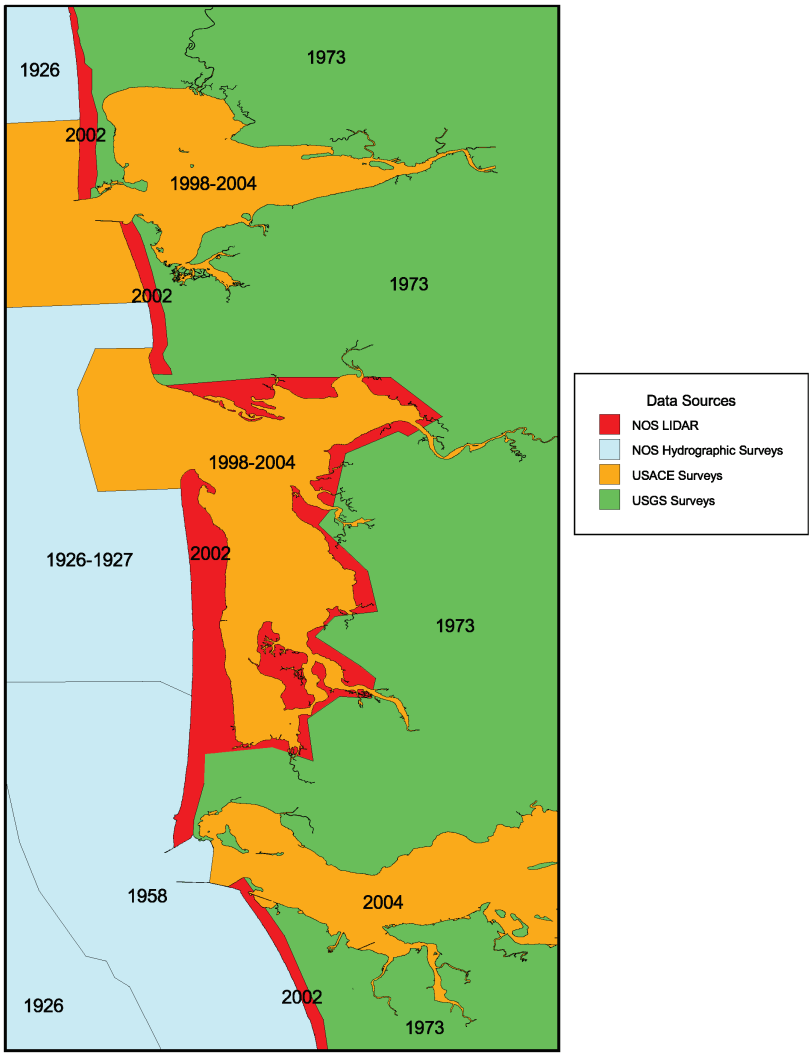

Figure 12: Coverage area of the primary data sources used in the high-resolution DEM. Sources are labeled with associated survey dates.

Table 5: Comparison of the MOST model and ADCIRC model simulations from Walsh *et al.* (2000). Figure 2 displays the locations of time series sites. Wave amplitudes are in meters.

	MOST model		ADCIRC model	
Time Series Site	**Max. crest**	**Max. trough**	**Max. crest**	**Max. trough**
1. Oyhut	5.6	10.0	N/A	N/A
2. Ocean Shores	6.3	9.3	4.7	6.4
3. Ocean Park	7.2	5.5	8.8	5.6
4. Oceanside	8.0	6.3	5.6	4.2
5. Seaview	7.2	6.1	5.5	3.7

Multiple data sources of various ages were used in the DEM (Fig. 12). Land elevations within the inundation grids are primarily based on recent high-resolution LIDAR surveys. U.S. Geological Survey (USGS) surveys from the 1970s were used to cover gaps in the topography. Bathymetric data were primarily taken from recent U.S. Army Corps of Engineers (USACE) surveys and much older NOS hydrographic surveys.

Though the DEM is based on the best available data in the region, it may not accurately reflect nearshore water depths. The age of the surveys in the nearshore coastal region are too old to reflect the significant changes of the Columbia River littoral zone. As described in the Study Area section, recent erosion trends have deepened the water offshore of these beach barriers. It is unclear how much error is introduced by using these older surveys. In order to accurately address this issue, high-resolution multibeam surveys should be conducted.

6.2 Model Comparison

This modeling study is an update to a prior effort that used a finite element model known as ADCIRC (Walsh *et al.*, 2000). Both studies used the same initial deformation scenario, but this study implements an updated DEM.

As discussed in previous sections, this study's high-resolution DEM includes very accurate LIDAR topography and updated bathymetry within the estuarine regions. The 2000 study used topography from 1973 USGS surveys (Priest *et al.*, 1997). The 6- to 10-m topographic contours from the USGS surveys do not cover the intricate details of the low-lying inundation areas. Significant coastal changes have also occurred along the barrier beaches over the past 30 years. Additionally, the 2000 DEM did not apply a standard vertical datum for all data sources leading to a 2- to 6-m vertical error range (Walsh *et al.*, 2000).

Table 5 shows the comparison between maximum wave crests and troughs based on specified time series locations (Fig. 2). The values for the ADCIRC model were estimated from graphics in Walsh *et al.* (2000). The MOST model produces higher maximum wave heights at all site locations except Ocean Park. Both studies predict that the first wave is the largest, and later waves occur at similar times.

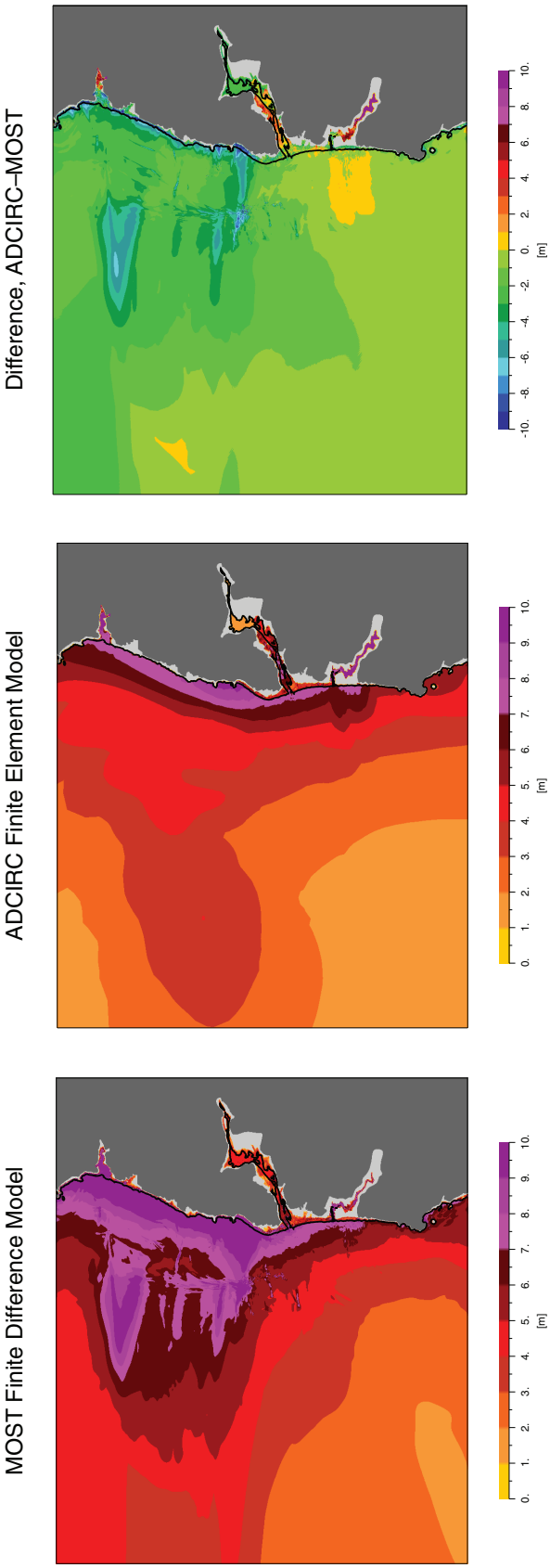

Figure 13: Comparison of MOST and ADCIRC model simulations for Gold Beach, Oregon. This model comparison was made in 2000 through a collaborative effort between the NOAA Center for Tsunami Inundation Mapping Efforts and the Oregon Graduate Institute of Science and Technology (unpublished material from NCTR archive).

Inundation patterns from Walsh *et al.* (2000) are not available for comparison. Instead, a comparison between the MOST and ADCIRC models is shown (Fig. 13) for a similar unpublished study at Gold Beach, Oregon. The higher maximum wave heights from the MOST model may be due to the higher resolution and better data quality of the B and C grids.

7. Conclusions and Recommendations for Future Work

This study modeled tsunami propagation and inundation along the southwest Washington coast based on a great M_w 9.1 CSZ earthquake with a local asperity. The results of this study (Appendix B) are being used to assess and enhance state mitigation efforts.

The results show extensive inundation in Ocean Shores and the Long Beach peninsula. High wave amplitudes and extreme currents are predicted across the Cascadia region. These results are similar to a prior modeling study by Walsh *et al.* (2000). Though the model produces reasonable maximum inundation patterns, a number of limitations lead to the following recommendations for future research:

- In this study, tides are assumed to interact linearly with the propagating tsunami. Thus, Mean High Water is used as the basis for the inundation model to obtain a reliable worst-case scenario. Further research is needed to incorporate tidal interactions into the model to produce more accurate wave heights and current speeds.

- The model uses reflective boundaries based on an offshore water depth in lower-resolution grids to maintain model stability. For this study, the reflection boundaries were over 750 m offshore in flat shallow regions near the coast. These barriers significantly impacted the amount of flow into estuarine regions and altered propagation patterns directly outside of the inundation area. Future improvements to the model should have more realistic reflection boundary depths (1–2 m) and account for instabilities due to seafloor baring in the propagation algorithm. Additionally the inundation region should include the estuaries to better assess the influence of propagation and dissipation in the intertidal zone.

- The model becomes unstable if computations of the flow become supercritical (Froude number >1). Given the local nature of the tsunami scenario and its associated intense wave speeds, supercritical flow on land is expected. Future versions of the model should handle supercritical flow scenarios by either incorporating its dynamics or limiting the computations to smaller Froude numbers. If the latter is chosen, then research should be conducted to analyze the effect of this limitation on near-field inundation. This is particularly important when considering

potential vertical evacuation strategies, such as calculating forces on structures.

- Multibeam bathymetric surveys should be conducted offshore of Washington and northern Oregon. This work could significantly reduce errors in the model and provide a better picture of seafloor changes in the Columbia River littoral cell.

- Prior work by Doyle (1996) suggest that abrupt tectonic subsidence from a large CSZ earthquake would cause 200–400 m of catastrophic beach retreat throughout the Columbia River littoral cell. An interesting research project would incorporate the modeled wave dynamics from this study with a shoreface translation model to determine the effect of tsunami waves on beach recession and subsequent alterations to sediment transport patterns within the littoral cell.

- This modeling study considered a credible worst-case scenario in the near field. After the devastating 26 December 2004 Boxing Day tsunami, many scientists have taken another look at the potential fault dynamics of the CSZ. Several new earthquake scenarios have been developed (Tsunami Pilot Study Working Group, 2006). Additional model scenarios should be run to determine whether the one used in this study remains the most credible worst case. Far-field scenarios are also being considered to help emergency managers consider potentially multiple evacuation strategies that are dependent on the event type.

Acknowledgments. This research was funded by the National Tsunami Hazard Mitigation Program via a grant from the Washington State Military Department Emergency Management Division. This publication is partially funded by the Joint Institute for the Study of the Atmosphere and Ocean (JISAO) under NOAA Cooperative Agreement No. NA17RJ1232, Contribution #1337.

The authors thank George Crawford, Tim Walsh, George Priest, and Lonnie Reid-Pell for assistance with data sources and processing. The authors also thank Hal Mofjeld and Mick Spillane for assisting with water-level datum issues and verifying the Gaussian distribution for the earthquake asperity. Utku Kânoğlu also expresses his gratitude to the Pacific Marine Environmental Laboratory for financial support during his summer 2005 visit.

8. References

Atwater, B.F. (1987): Evidence for great Holocene earthquakes along the outer coast of Washington State. *Science, 336*, 942–944.

Atwater, B.F., A.R. Nelson, J.J. Clague, G.A. Carver, D.K. Yamaguchi, P.T. Bobrowski, J. Bourgeois, M.E. Darienzo, W.C. Grant, E. Hemphill-Haley, H.M. Kelsey, G.C. Jacoby, S.P. Nishenko, S.P. Palmer, C.D. Peterson, and M.A. Reinhart (1995): Summary of coastal geologic evidence for past great earthquakes at the Cascadia subduction zone. *Earthq. Spectra, 11*(1), 1–18.

Doyle, D.L. (1996): Beach response to subsidence following a Cascadia subduction zone earthquake along the Washington-Oregon coast. M.S. thesis, Portland State University, Portland, OR, 113 pp.

Goldfinger, C., L.D. Kulm, R.S. Yeats, C. Mitchell, R.E. Weldon, III, C.D. Peterson, M.E. Darienzo, W. Grant, and G. Priest (1992): Neotectonic map of the Oregon continental margin and adjacent abyssal plain. Oregon Department of Geology and Mineral Industries Open-File Report O-92-4, 17 pp.

Grays Harbor County (2005): Grays Harbor County statistical information. `http://www.co.grays-harbor.wa.us/`

Kaminsky, G.M., M.C. Buijsman, G. Gelfenbaum, P. Ruggiero, H.M. Jol, A.E. Gibbs, and C.D. Peterson (1999): Synthesizing geological observations and processes-response data for modeling coastal change at management scale. In *Proceedings of Coastal Sediments 99*, ASCE, 1708–1723.

Mofjeld, H.O., M.G.G. Foreman, and A. Ruffman (1997): West Coast tides during Cascadia Subduction Zone tsunamis. *Geophys. Res. Lett., 24*(17), 2215–2218.

Mofjeld, H.O., F.I. González, V.V. Titov, A.J. Venturato, and J.C. Newman (2007): Effects of tides on maximum tsunami wave heights: Probability distributions. *J. Atmos. Ocean. Tech., 24*(1), 117–123.

Mofjeld, H.O., V.V Titov, F.I. González , and J.C. Newman (2000): Analytic theory of tsunami wave scattering in the open ocean with application to the North Pacific. NOAA Tech. Memo. OAR PMEL-116, NTIS: PB2002-101562, NOAA/Pacific Marine Environmental Laboratory, Seattle, WA, 38 pp.

Mofjeld, H.O., A.J. Venturato, F.I. González , and V.V. Titov (2004): Background tides and sea level variations at Seaside, Oregon. NOAA Tech. Memo. OAR PMEL-126, NTIS: PB2005-100990, NOAA/Pacific Marine Environmental Laboratory, Seattle, WA, 15 pp.

Myers, E.P., III, A.M. Baptista, and G.R. Priest (1999): Finite element modeling of potential Cascadia subduction zone tsunamis. *Science of Tsunami Hazards, 17*(1), 3–18.

National Science and Technology Council (2005): Tsunami risk reduction for the United States: A framework for action. Joint Report of the Subcommittee on Disaster Reduction and the U.S. Group on Earth Observations, 30 pp.

Ocean Shores Chamber of Commerce (2005): Ocean Shores Visitor Guide, Ocean Shores, Washington. `http://oceanshores.org/`

Pacific County (2003): Pacific County statistical information. `http://www.co.pacific.wa.us/`

Petersen, M.D., C.H. Cramer, and A.D. Frankel (2002): Simulations of seismic hazard for the Pacific Northwest of the United States from earthquakes associated with the Cascadia subduction zone. *Pure Appl. Geophys., 159*(9), 2147–2168.

Peterson, C.D., G. Gelfenbaum, H.M. Jol, J.B. Phipps, F. Reckendorf, D.C. Twichell, S. Vanderburgh, and L. Woxell (1999): Great earthquakes, abundant sand, and

high wave energy in the Columbia cell, USA. In *Proceedings of Coastal Sediments 99*, ASCE, 1676–1691.

Priest, G.R., E.P. Myers III, A.M. Baptista, P. Fleuck, K. Wang, R.A. Kamphaus, and C.D. Peterson (1997): Cascadia subduction zone tsunamis—Hazard mapping at Yaquina Bay, Oregon. Oregon Department of Geology and Mineral Industries Open-File Report O-97-34, 144 pp.

Satake, K., K. Shimazaki, Y. Tsuji, and K. Ueda (1996): Time and size of a great earthquake in Cascadia inferred from Japanese tsunami records of January 1700. *Nature, 379*(6562), 246–249.

Synolakis, C.E., E.N. Bernard, V.V. Titov, U. Kânoğlu, and F.I. González (2007): Standards, criteria, and procedures for NOAA evaluation of tsunami numerical models. NOAA Tech. Memo. OAR PMEL-135, NOAA/Pacific Marine Environmental Laboratory, Seattle, WA, 55 pp.

Titov, V.V., and F.I. González (1997): Implementation and testing of the Method of Splitting Tsunami (MOST) model. NOAA Tech. Memo. ERL PMEL-112, NTIS: PB98-122773, NOAA/Pacific Marine Environmental Laboratory, Seattle, WA, 11 pp.

Titov,V.V., F.I. González, H.O. Mofjeld, and A.J. Venturato (2003): NOAA TIME Seattle tsunami mapping project: Procedures, data sources, and products. NOAA Tech. Memo. OAR PMEL-124, NTIS: PB2004-101635, NOAA/Pacific Marine Environmental Laboratory, Seattle, WA, 21 pp.

Titov, V.V., and C.E. Synolakis (1998): Numerical modeling of tidal wave runup. *J. Waterw. Port Coast. Ocean Eng., 124*(4), 157–171.

Tsunami Pilot Study Working Group (2006): Seaside, Oregon Tsunami Pilot Study—Modernization of FEMA flood hazard maps. NOAA OAR Special Report, NOAA/OAR/PMEL, Seattle, WA, 94 pp.

Venturato, A.J. (2005): A digital elevation model for Seaside, Oregon: Procedures, data sources, and analyses. NOAA Tech. Memo. OAR PMEL-129, NTIS: PB2006-101562, NOAA/Pacific Marine Environmental Laboratory, Seattle, WA, 17 pp.

Walsh, T.J., C.G. Caruthers, A.C. Heinitz, E.P. Myers III, A.M. Baptista, G.B. Erdakos, and R.A. Kamphaus (2000): Tsunami hazard map of the southern Washington Coast: Modeled tsunami inundation from a Cascadia subduction zone earthquake. Washington Division of Geology and Earth Resources Geologic Map GM-49, 3–12.

Washington State Department of Ecology (2007): Washington State Coastal Hazards. `http://www.ecy.wa.gov/programs/sea/coast/hazards.html`

Wells, R.E., R.J. Blakely, Y. Sugiyama, D.W. Scholl, and P.A. Dinterman (2003): Basin-centered asperities in great subduction zone earthquakes: A link between slip, subsidence, and subduction erosion? *J. Geophys. Res., 108*(B10), 2507–2537.

Woxell, L.K. (1998): Prehistoric beach accretion rates and long-term response to sediment depletion in the Columbia River Littoral System, USA. M.S. thesis, Portland State University, Portland, OR, 206 pp.

Yamaguchi, D.K., B.F. Atwater, D.E. Bunker, B.E. Benson, and M.S. Reid (1997): Tree-ring dating in the 1700 Cascadia earthquake. *Nature, 389*(6654), 922–924.

Appendix A: Data Credit

NOAA Coastal Services Center, Coastal Remote Sensing Program (2004): Aircraft Laser/GPS mapping of coastal topography. Charleston, South Carolina. http://www.csc.noaa.gov/lidar/

NOAA National Geodetic Survey (2004): Vertical geodetic control data. Silver Spring, Maryland. http://www.ngs.noaa.gov/

NOAA National Geophysical Data Center (2002): NOS Hydrographic Database, GEODAS Version 4.1.18. Boulder, Colorado. http://ngdc.noaa.gov/

NOAA National Ocean Service (2004): Regional water-level station benchmarks. Silver Spring, Maryland. http://tidesandcurrents.noaa.gov/benchmarks/

Oregon Bureau of Land Management (2001): Oregon Watershed Boundaries. Portland, Oregon. Data obtained through the Oregon Geospatial Data Clearinghouse. http://www.gis.state.or.us/

U.S. Army Corps of Engineers (2004): Hydrographic surveys for Columbia River, Grays Harbor, and Willapa Bay. Portland, Oregon and Seattle, Washington. http://www.nwp.usace.army.mil/

U.S. Geological Survey EROS Data Center (1999): National Elevation Dataset. Sioux Falls, South Dakota. http://gisdata.usgs.net/ned/

U.S. Geological Survey National Aerial Photography Program (2002): 2000 Digital Orthophoto Quads. Reston, Virginia. Data obtained through the Oregon Geospatial Data Clearinghouse. http://www.gis.state.or.us/

Washington State Department of Ecology (2001): Washington State marine shorelines. Olympia, Washington. http://www.ecy.wa.gov/services/gis/

Appendix B: Modeling Products

Model results (Table B.1) were provided to two Washington State agencies, the Military Department Emergency Management Division and the Division of Geology and Earth Resources, for use in tsunami hazard mapping and mitigation. All geospatial data were provided in ASCII raster or ESRI ArcGIS© formats. Animations were provided in QuickTime© format. These state agencies are responsible for redistribution of these data.

Table B.1: Tsunami model products.

Name	**Type**
animations	QuickTime movies depicting tsunami wave evolution and amplitudes
documentation	Modeling product report and presentations
gis	Geospatial representation of model results and DEMs in ESRI ArcGIS©and ASCII raster formats
images	Images of model results
metadata	Information related to each dataset
timeseries	Spreadsheet of model time series for specific sites along the Washington coast